Scale sensitivity of the Gill circulation, Part II: off-equatorial case

Gilles Bellon[1] and Beatriz Reboredo[1]

[1]University of Auckland

November 22, 2022

Abstract

We investigate the steady dynamical response of the atmosphere on the equatorial β-plane to a steady, localized, mid-tropospheric heating source. Following Part I which investigated the case of an equatorial diabatic heating, we explore the sensitivity of the Gill circulation to the latitudinal location of the heating, together with the sensitivity to its horizontal scale. Again, we focus on characteristics of the response which would be particularly important if the circulation interacted with the hydrologic and energy cycles. In the off-equatorial case, the intensity of the overturning circulation has the same limit as in the equatorial case for small horizontal extent of the diabatic heating, which is also the limit in the non-rotating case and the f-plane case. The decrease in this intensity with increasing horizontal scale of the diabatic heating is slightly faster in the off-equatorial case than in the equatorial case, but slower than in the f-plane case, which shows that the β effect disrupts the rotational motion.

The low-level westerly jet is more intense than in the equatorial case, with larger maximum wind and eastward mass transport that tend to infinity for small horizontal extent of the diabatic heating. While the latitudinal extent of the jet is not very sensitive to the latitude of the diabatic heating, it is not symmetric with respect to the latitude of the diabatic-heating center, unlike in the equatorial case: it extends further equatorward than poleward of the diabatic-heating center. It also extends further eastward than in the equatorial case.

Scale sensitivity of the Gill circulation, Part II: off-equatorial case

Gilles Bellon [1], Beatriz Reboredo [1]

[1]Department of Physics, University of Auckland, Auckland, New Zealand.

Key Points:

- The off-equatorial circulation exhibits a weaker overturning circulation than the equatorial circulation except for a localized heating.
- This circulation exhibits a faster low-level westerly jet than the equatorial circulation, particularly for a localized heating.
- The low-level westerly jet is asymmetric with respect to the latitude of the heating, extending further equatorward than poleward.

Corresponding author: Gilles Bellon, `gilles.bellon@auckland.ac.nz`

Abstract

We investigate the steady dynamical response of the atmosphere on the equatorial β-plane to a steady, localized, mid-tropospheric heating source. Following Part I which investigated the case of an equatorial diabatic heating, we explore the sensitivity of the Gill circulation to the latitudinal location of the heating, together with the sensitivity to its horizontal scale. Again, we focus on characteristics of the response which would be particularly important if the circulation interacted with the hydrologic and energy cycles. In the off-equatorial case, the intensity of the overturning circulation has the same limit as in the equatorial case for small horizontal extent of the diabatic heating, which is also the limit in the non-rotating case and the f-plane case. The decrease in this intensity with increasing horizontal scale of the diabatic heating is slightly faster in the off-equatorial case than in the equatorial case, but slower than in the f-plane case, which shows that the β effect disrupts the rotational motion. The low-level westerly jet is more intense than in the equatorial case, with larger maximum wind and eastward mass transport that tend to infinity for small horizontal extent of the diabatic heating. While the latitudinal extent of the jet is not very sensitive to the latitude of the diabatic heating, it is not symmetric with respect to the latitude of the diabatic-heating center, unlike in the equatorial case: it extends further equatorward than poleward of the diabatic-heating center. It also extends further eastward than in the equatorial case.

Plain Language Summary

While Part I focuses on the dynamical response to steady diabatic heating at the equator, this study investigates the influence of the latitude of the diabatic heating on the characteristics of the circulation. For the same finite horizontal extent of diabatic heating, the dynamical response to off-equatorial diabatic heating has a weaker overturning circulation than in the equatorial case. Low-level westerly winds are also stronger for off-equatorial diabatic heating than in the equatorial case, and they are located equatorward of the heating center. Our results suggest a more complex coupling of the circulation with the energy and water cycle in the off-equatorial case than in the equatorial case: this coupling would result in feedbacks with larger amplitudes for an off-equatorial diabatic heating than for an equatorial heating, but less colocated with the initial forcing.

1 Introduction

Gill (1980, hereafter G80)'s seminal work showed that the damped, linear, baroclinic dynamical response of the tropical atmosphere to a localized, steady, mid-tropospheric diabatic heating reproduces the main features of tropical circulations. G80's study aimed to provide a very simple model of the Walker circulation resulting from equatorial regional diabatic heating as well as monsoon circulations resulting from off-equatorial heating. Indeed, monsoon circulations exhibit distinct features compared to circulations in response to equatorial forcing, and in particular a change of direction of low-level winds forming a monsoon jet (Ramage, 1971; Joseph & Raman, 1966) which significantly affects the hydrologic cycle.

In the context of slow intraseasonal oscillations (30-60 days), for which the circulation can be considered in quasi-equilibrium with the diabatic heating, the off-equatorial Gill circulation is particularly relevant to the monsoon intraseasonal oscillation (also called northward-propagating, boreal-summer intraseasonal oscillation, see Goswami, 2005, for a review). Although the main mechanisms of this intraseasonal oscillation are still debated (Jiang et al., 2004; Bellon & Srinivasan, 2006; Bellon & Sobel, 2008a; Boos & Kuang, 2010; Kang et al., 2010; Sharmila et al., 2013; Gao et al., 2019), moisture-convergence feedback and wind-induced surface heat fluxes are expected to play major roles in the development and propagation of the convective disturbances. A better theoretical understanding of the off-equatorial Gill circulation is therefore useful to improve our grasp of the dynamical features susceptible to impact these feedbacks.

G80 focused on two cases: the simplest case with diabatic heating symmetric about the equator and the simplest case with diabatic asymmetric about the equator. G80 considered that the monsoon circulation was well represented by the sum of these two cases; but monsoon circulations are probably better depicted by the dynamical response of the tropical atmosphere to a simple off-equatorial diabatic heating rather than by the response to this sum of two heating patterns (Wu et al., 2009), and extending G80's work to study this response is the motivation of this article. We base a lot of the present work's derivations and results on those in Reboredo and Bellon (2020, hereafter Part I), in which we looked at the sensitivity of the Gill circulation to the latitudinal and longitudinal extents of an equatorial diabatic heating.

In Section 2, we present some specifics of the off-equatorial case on the equatorial β-plane and the solutions on a local f-plane. Section 3 presents some solutions as well as the scale sensitivity of the overturning circulation and of the low-level wind to the size and location of the diabatic heating. Section 4 summarizes our findings and concludes.

2 Method

We use the analytical results of Part I (Sections 2.1 and 2.2), and we apply them to a more general diabatic heating distribution, with the same shape but centered on a latitude y_0 rather than systematically on the equator:

$$Q = F(x)D(y), \tag{1}$$

with:

$$F(x) = \begin{cases} k\cos(kx) & \text{for } |x| < L_x, \\ 0 & \text{for } |x| > L_x, \end{cases} \text{ with } k = \frac{\pi}{2L_x}, \tag{2}$$

$$D(y) = \frac{1}{L_y}\exp\left(-\frac{(y-y_0)^2}{4L_y^2}\right). \tag{3}$$

The case $y_0 = 0$ is the focus of Part I, and similarly the heating pattern is close to circular for $L_x = 3L_y$. Again, the total heating (or total energy input) imposed to the atmosphere is independent of the longitudinal and latitudinal scales:

$$[Q] = 4\sqrt{\pi}, \tag{4}$$

with the brackets $[\cdot]$ indicating global integration.

As in Part I, D can be decomposed in a series on the basis of cylinder functions $(D_n)_{n\in\mathbb{N}}$:

$$\begin{aligned} D(y) &= \sum_{n=0}^{\infty} a_n(L_y, y_0) D_n(y), \\ \text{with } a_0 &= \sqrt{\frac{2}{L_y^2+1}} \exp\left(-\frac{y_0^2}{4(L_y^2+1)}\right), \\ a_1 &= \frac{y_0\, a_0}{L_y^2+1}, \\ \text{and } a_n &= \frac{y_0\, a_{n-1} + (L_y^2-1)\, a_{n-2}}{n\,(L_y^2+1)} \text{ for } n > 1. \end{aligned} \tag{5}$$

$$\tag{6}$$

Indeed, for $y_0 = 0$, this expression of a_n reduces to the expressions of a_{2n} and a_{2n+1} given in Part I.

As shown in Part I, the solution to Gill's steady, linear equation system forced by diabatic heating $Q = F(x)D(y)$ can be written as an infinite sum (see Eqs. (38)-(40) in Part I) of the solutions $(T^{(n)}, u^{(n)}, v^{(n)})$ to the diabatic heatings $Q^{(n)} = F(x)D_n(y)$ (see Eqs. (24)-(31) in Part I). In practice, we approximate the infinite sum by a finite sum up to a value $n = m$ set by a convergence criterion (Cauchy, 1821, see Part I). As for the vertical speed, it can be obtained using $w = Q - \epsilon T = \partial_x u + \partial_y v$.

2.1 A baseline: the f-plane case

As in Part I, we can compare the Gill circulation to the case with uniform effect of rotation, i.e. on an f plane with the value of f determined by the latitude of the center of the diabatic heating y_0: $f = y_0/2$. The system reduces to a damped inertio-gravity wave. Equations (4) and (5) from Part I reduce to:

$$w = -\frac{\epsilon}{\epsilon^2+f^2}\Delta T, \tag{7}$$

$$T = \frac{1}{\epsilon}Q + \frac{1}{\epsilon^2+f^2}\Delta T. \tag{8}$$

Again, the vertical energy transport associated with the circulation appears as a diffusive term that modulates the direct thermodynamic response Q/ϵ, as in the non-rotating case ($f = 0$) presented in Part I. Also, the large-scale transport damps temperature gradients, and the equilibrium temperature response to a diabatic heating is spatially smoother than the diabatic heating itself. Compared to the non-rotating case ($f = 0$), this diffusive term is smaller, and the temperature response therefore less smooth. The effect of rotation creates a baroclinic, cyclonic circulation around temperature maxima, additionally to the divergent flow:

$$u = -\frac{\epsilon}{\epsilon^2+f^2}\frac{\partial T}{\partial x} - \frac{f}{\epsilon^2+f^2}\frac{\partial T}{\partial y}, \tag{9}$$

$$v = -\frac{\epsilon}{\epsilon^2+f^2}\frac{\partial T}{\partial y} + \frac{f}{\epsilon^2+f^2}\frac{\partial T}{\partial x}, \tag{10}$$

in which the first term on the right-hand side is the divergent component of the wind ans the second is the rotational component, and it is straightforward that these components are perpendicular.

The damped inertio-gravity wave response to a forcing described by Equation (1) can be obtained by using the Fourier decomposition of the latitudinal dependence of Q; if we have:

$$D(y) = \frac{1}{\sqrt{\pi}} \int_{-\infty}^{+\infty} \cos(\ell y')\, e^{-\ell^2 {L_y}^2}\, d\ell, \tag{11}$$

with y' the latitudinal coordinate with the origin at the center of the diabatic heating: $y' = y - y_0$; as in the non-rotating case in Part I, we can write the equilibrium temperature response as a Fourier decomposition:

$$T = \frac{1}{\sqrt{\pi}} \int_{-\infty}^{+\infty} \mathcal{T}_\ell(x)\, \cos(\ell y')\, e^{-\ell^2 {L_y}^2}\, d\ell, \tag{12}$$

each function $\mathcal{T}_\ell$ is solution to:

$$\lambda^2 \mathcal{T}_\ell - \partial_{xx}\mathcal{T}_\ell = \frac{\epsilon^2 + f^2}{\epsilon} F(x), \tag{13}$$

with $\lambda^2 = \left(\epsilon^2 + f^2 + \ell^2\right)$. This second-order linear differential equations can be solved for $x < -L_x$, $|x| < L_x$, and $x > L_x$. The solutions to the corresponding homogeneous equation are $e^{\pm\lambda x}$, and a particular solution proportional to $\cos(kx)$ for $|x| < L_x$ is easily found. By using continuity conditions at $x = \pm L_x$ and evanescent conditions for $x \longrightarrow \pm\infty$, the general solution can be derived:

$$\frac{\lambda^2 + k^2}{\epsilon^2 + f^2}\, \mathcal{T}_\ell \ = \begin{cases} \frac{k}{\epsilon}\cos(kx) + \frac{k^2}{\epsilon\lambda}\, e^{-\lambda L_x} \cosh(\lambda x) & \text{if } |x| < L_x, \\ \frac{k^2}{\epsilon\lambda}\cosh(\lambda L_x)\, e^{-\lambda|x|} & \text{if } |x| > L_x. \end{cases} \tag{14}$$

The corresponding winds can be decomposed via Fourier decomposition as well:

$$\begin{aligned} u &= \frac{1}{\sqrt{\pi}} \int_{-\infty}^{+\infty} \left[\mathcal{U}_\ell^\delta(x)\, \cos(\ell y') + \mathcal{U}_\ell^\zeta(x)\, \sin(\ell y')\right] e^{-\ell^2 {L_y}^2}\, d\ell, \\ v &= \frac{1}{\sqrt{\pi}} \int_{-\infty}^{+\infty} \left[\mathcal{V}_\ell^\delta(x)\, \sin(\ell y') + \mathcal{V}_\ell^\zeta(x)\, \cos(\ell y')\right] e^{-\ell^2 {L_y}^2}\, d\ell, \\ w &= \frac{1}{\sqrt{\pi}} \int_{-\infty}^{+\infty} \mathcal{W}_\ell(x)\, \cos(\ell y')\, e^{-\ell^2 {L_y}^2}\, d\ell, \end{aligned} \tag{15}$$

with

$$\left(\lambda^2 + k^2\right) \mathcal{U}_\ell^\delta \ = \begin{cases} k^2 \sin(kx) - k^2 e^{-\lambda L_x} \sinh(\lambda x) & \text{if } |x| < L_x, \\ \mathrm{sgn}(x) k^2 \cosh(\lambda L_x)\, e^{-\lambda|x|} & \text{if } |x| > L_x, \end{cases} \tag{16}$$

$$\mathcal{U}_\ell^\zeta = \frac{f\ell}{\epsilon^2 + f^2}\mathcal{T}_\ell, \tag{17}$$

$$\mathcal{V}_\ell^\delta = \frac{\epsilon}{f}\mathcal{U}_\ell^\zeta, \tag{18}$$

$$\mathcal{V}_\ell^\zeta = -\frac{f}{\epsilon}\mathcal{U}_\ell^\delta, \tag{19}$$

and

$$\frac{\lambda^2 + k^2}{\epsilon^2 + f^2}\, \mathcal{W}_\ell \ = \begin{cases} \frac{\ell^2 + k^2}{\epsilon^2 + f^2} k\cos(kx) - \frac{k^2}{\lambda}\, e^{-\lambda L_x} \cosh(\lambda x) & \text{if } |x| < L_x, \\ -\frac{k^2}{\lambda}\cosh(\lambda L_x)\, e^{-\lambda|x|} & \text{if } |x| > L_x. \end{cases} \tag{20}$$

The superscripts "δ" and "ζ" indicates, respectively, the divergent and rotational components of the horizontal wind.

Compared to the case without effect of the Earth rotation ($f = 0$, the damped gravity wave presented in Part I), each contribution $\mathcal{T}_\ell$ is larger, so the total temperature anomalies will be larger, but the exponential decay of the anomalies outside the heating region is faster. This results from a weaker redistribution by transport due to a slower vertical speed resulting from a smaller divergent component of the wind. The rotational component of the wind increases with f (it is zero in the non-rotating case, for $f = 0$).

2.2 Limits for small zonal extent of the heating

Here, we explore the asymptotic solutions for $L_x \to 0$, focusing on the interval $-L_x \leq x \leq L_x$. Outside this interval, there is no simple expression for the infinite sums or integrals of exponentially decreasing modes which are solutions. Qualitatively, there is subsidence outside of $[-L_x, L_x]$ in both the β-plane and the f-plane cases.

Damped inertio-gravity wave:

For $L_x \to 0$, $k \to +\infty$, and

$$\mathcal{T}_\ell \sim \tfrac{\epsilon^2+f^2}{\epsilon\lambda}, \tag{21}$$

$$\begin{aligned} \mathcal{U}_\ell^\delta &\sim \sin kx, \qquad \mathcal{U}_\ell^\zeta \sim \frac{f\ell}{\epsilon\lambda}, \\ \mathcal{V}_\ell^\delta &\sim \tfrac{\ell}{\lambda}, \qquad \mathcal{V}_\ell^\zeta \sim -\frac{f}{\epsilon}\sin kx, \\ \mathcal{W}_\ell &\sim k\cos kx. \end{aligned} \tag{22}$$

It follows through the inverse Fourier transforms that:

$$u^\delta \sim \sin(kx)\, D(y), \tag{23}$$

$$w \sim k\cos(kx)\, D(y) = Q, \tag{24}$$

i.e., at first order the Newtonian cooling is negligible in front of the diabatic heating and advective cooling. The ascending region is therefore the same as the diabatic heating region. And the divergence is dominated by the contribution of the zonal wind: $w \sim \partial_x u^\delta$.

Off-equatorial Gill circulation:

Equations (58)-(61) established in Part I are valid for all latitudinal distribution D of diabatic heating:

$$T \sim \frac{1}{2}(1-\sin kx)\; y^2\, D(y) + a_0 D_0(y), \tag{25}$$

$$u \sim -2(1-\sin kx)\left[D(y) + \frac{y}{2}\frac{dD}{dy}\right] + a_0 D_0(y), \tag{26}$$

$$v \sim -k\cos(kx)\, y\, D(y), \tag{27}$$

$$w \sim k\cos(kx)\, D(y) \sim Q, \tag{28}$$

for $|x| < L_x$ in the limit $L_x \to 0$.

In the case of an off-equatorial Gaussian (Eq. (3)) of interest here, and in the limit $L_y \to 0$, we can simplify the expression for the zonal wind:

$$u \sim -2(1-\sin kx)\left[1 - \frac{y(y_0-y)}{4L_y^2}\right] D(y) + a_0 D_0(y), \tag{29}$$

2.3 Additional experiments

As in Part I, we also used both a linear and a non-linear versions of the QTCM on a β-plane (Sobel & Neelin, 2006; Bellon & Sobel, 2008b, 2010; Bellon, 2011) reduced to its baroclinic structure to verify our results by integrating the simplified QTCM in time from an initial state of rest until it reaches a steady state (after about 15 days of simulation). With both the linear and non-linear, simplified QTCM versions, we obtained very similar results to our analytical derivations, which gives us high confidence in our results. In particular, the similarity of these simulations with the semi-analytical solutions confirms the validity of the longwave approximation and the fact that the linear system behaves like the non-linear, energy-conserving system within a realistic range of forcing. The differences between these additional experiments and our semi-analytical results are so small (below 2%) that we only present our analytical work in the following section.

3 Results

3.1 Temperature and wind response

We present here the features of the solutions in terms of temperature, surface winds and mid-tropospheric vertical motion for a few cases with diabatic heatings of different horizontal extents centered away from the equator, for both the f-plane case (damped inertio-gravity wave) and the equatorial β-plane case (Gill circulation). In all cases, the horizontally integrated heating $[Q]$ is the same. Figure 1 depicts contours of temperature perturbation and surface velocity field for the damped inertio-gravity wave forced by heating with meridional scale $L_y = 1$ (one equatorial radius of deformation, Fig. 1a,c) and $L_y = 1/2$ (Fig. 1b,d), centered at $y_0 = 1$ (Fig. 1a,b) and $y_0 = 2$ (Fig. 1c,d).Figure 2 shows the corresponding contours of mid-tropospheric vertical velocity together with contours of heating. Figures 1a,b and 2a,b in Part I show the corresponding figures for the same pattern of diabatic heating centered at the equator (y_0=0). Figures 3 and 4 show the same fields for the Gill circulation (i.e., on the β-plane) forced by the same diabatic heating distributions. Figures 3a,b and 4a,b in Part I show the corresponding figures for the same pattern of diabatic heating centered at the equator (y_0=0).

In all cases, we set $L_x = 3L_y$ so that isolines of diabatic heating are close to circular near its maximum. We have investigated cases with different ratios L_x/L_y and found that the sensitivity of the off-equatorial Gill circulation to the aspect ratio of the diabatic-heating region is similar to the equatorial case discussed in Part I; in particular, the relative sensitivity of the global metrics of the circulation (intensities of the overturning circulation and the low-level westerly jet) to the latitude of the heating center is almost independent of the aspect ratio of the diabatic-heating region. We show the main results for $L_x = 1.5L_y$ and $L_x = 6L_y$ in Appendix A, and we will focus on the case $L_x = 3L_y$ in the main text of this article.

The damped inertio-gravity wave exhibits a near-circular, warm mid-tropospheric temperature perturbation collocated with the heating, which forces a cyclonic gyre with surface wind essentially tangent to the isolines of temperature (Fig. 1). This shows that the flow is mostly rotational and almost geostrophic. Still, there is a divergent component to the horizontal flow that results in ascent almost collocated with the heating (Fig. 2). The solution of the β-plane differs significantly, from the f-plane solutions: the off-equatorial Gill circulation exhibits a strong rotational gyre, but it is located poleward and westward of the diabatic heating, and not as circular; the Gill circulation also exhibits Kelvin-wave easterlies east of the heating and a weak cyclonic gyre in the other hemisphere (Fig. 3). Compared to the equatorial case (Fig. 3a,b in Part I), the gyre next to the heating is faster and a stronger westerly jet develops between the equator and the center of the diabatic heating, similar to the observed monsoon jets; the Kelvin-wave easterlies and the gyre in the other hemisphere are weaker.

As expected, the temperature and wind fields are symmetric in latitude and longitude for the damped inertio-gravity wave (Figs. 1 and 2), while the symmetry is bro-

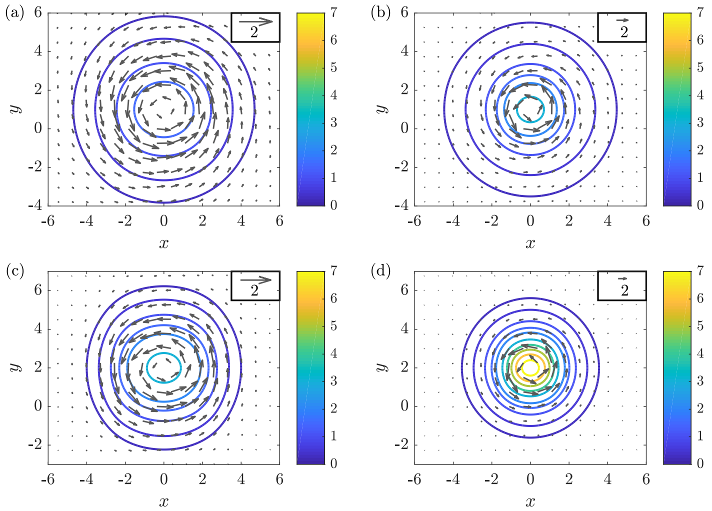

Figure 1: Solutions for the damped inertio-gravity wave (f-plan case): (non-dimensional) temperature response (contours) and low-level velocity (vectors) for (a) $(y_0, L_y) = (1, 1)$, (b) $(y_0, L_y) = (1, 1/2)$, (c) $(y_0, L_y) = (2, 1)$, and (d) $(y_0, L_y) = (2, 1/2)$; in all cases, $L_x = 3L_y$; temperature contours are at (0.25, 0.5, 1, 1.5, 2, 3, 4, 5, 6, 7).

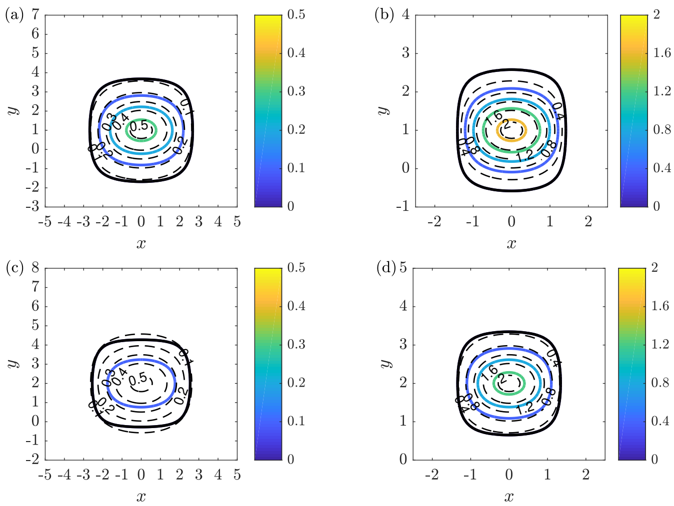

Figure 2: Forcing and solution for the damped inertio-gravity wave (f-plan case): diabatic heating (dashed contours) and mid-tropospheric vertical velocity (solid contours) for (a) $(y_0, L_y) = (1, 1)$, (b) $(y_0, L_y) = (1, 1/2)$, (c) $(y_0, L_y) = (2, 1)$, and (d) $(y_0, L_y) = (2, 1/2)$; in all cases, $L_x = 3L_y$. Contour spacing: 0.1 in (a) and (c), 0.4 in (b) and(d); black for $w = 0$.

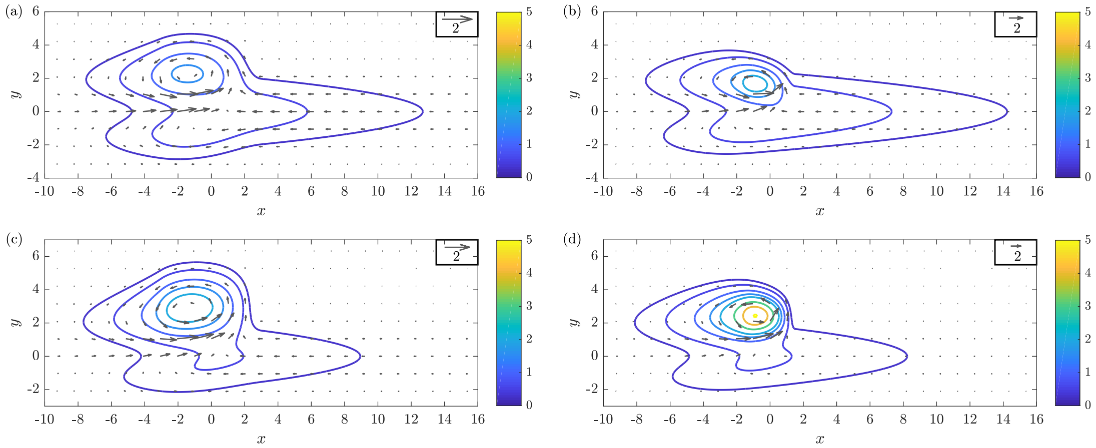

Figure 3: Solutions for the Gill circulation: (non-dimensional) temperature response (contours) and low-level velocity (vectors) for (a) $(y_0, L_y) = (1, 1)$, (b) $(y_0, L_y) = (1, 1/2)$, (c) $(y_0, L_y) = (2, 1)$, and (d) $(y_0, L_y) = (2, 1/2)$; in all cases, $L_x = 3L_y$; temperature contours are at (0.25, 0.5, 1, 1.5, 2, 3, 4, 5, 6, 7).

ken in the Gill circulation (Figs. 3 and 4) due to the change of Coriolis parameter with latitude.

As the latitude of the diabatic heating y_0 is increased, the damped-inertio-gravity-wave gyre moves poleward and becomes faster, and the temperature maximum increases (Fig. 1), by one order of magnitude compared to the non-rotating case presented in Part I (which corresponds to the equatorial f-plane case, for $y_0 = 0$). Figure 2 shows that upward motion, and therefore the divergent component of the horizontal wind, decreases with a poleward displacement of the diabatic heating. Advective cooling by ascent, which damps the temperature perturbation in the diabatic-heating region, decreases with this slowing of the upward motion, which explains the much larger temperature anomaly. This is consistent with the diffusive effect of vertical energy transport on temperature perturbation and its scaling in $(\epsilon^2 + f^2)^{-1}$ discussed in Section 2.1 that yields a decrease with increasing y_0. The rotational wind scales with $f/(\epsilon^2 + f^2)$, while the divergent wind scales with $\epsilon/(\epsilon^2 + f^2)$ (see Eqs. (9)-(10)), which explains the increase in the speed of the gyre with increasing y_0, and the decrease in ascending motion. We can also follow the same energy reasoning as in Part I, since energy conservation appears well approximated by the linear system (see Section 2.3): in our equation system, thermal energy and kinetic energy have the same dissipation rate ϵ and the only source of energy is the imposed diabatic heating; the global energy (i.e., sum of thermal and kinetic energy integrated over the whole atmosphere) is therefore set by $[Q]/\epsilon$. This means that the larger the solution's temperature perturbation, the larger the share of global energy in the thermal reservoir and the smaller the solution's kinetic energy. In the damped inertio-gravity wave, the rotational and divergent winds are perpendicular, which means that the kinetic energy can be decomposed in the sum of a rotational-wind component and a divergent-wind component, each proportional to the square of the corresponding wind. For a given kinetic energy, the larger the rotational component, the smaller the divergent component. The ratio between the amplitudes of the rotational and divergent wind is f/ϵ (see Eqs. (9)-(10)), which shows that the fraction of kinetic energy that is due to rotational wind increases in f^2. Indeed, an increase in the effect of rotation (i.e., an increase in f $= y_0/2$) increases the rotational wind and therefore the fraction of the global energy stored as rotational kinetic energy. This reduces the divergent kinetic energy, the divergent wind, and the associated vertical motion. As a result, the advective cooling is less efficient at

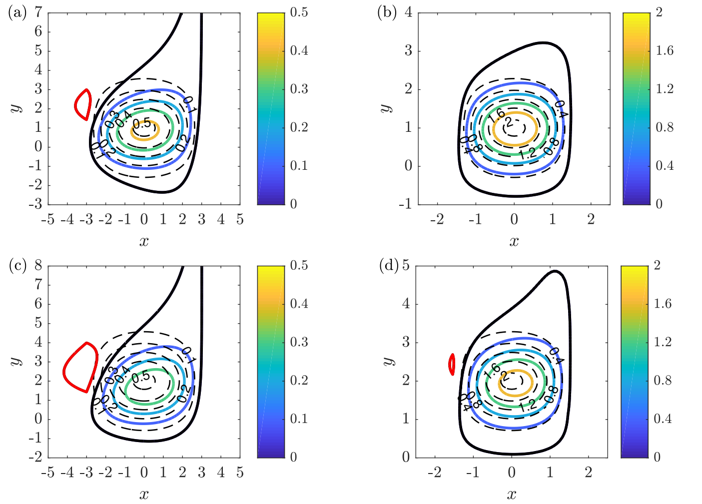

Figure 4: Forcing and solution for the Gill circulation: diabatic heating (dashed contours) and mid-tropospheric vertical velocity (solid contours) for (a) $(y_0, L_y) = (1, 1)$, (b) $(y_0, L_y) = (1, 1/2)$, (c) $(y_0, L_y) = (2, 1)$, and (d) $(y_0, L_y) = (2, 1/2)$; in all cases, $L_x = 3L_y$. Contour spacing: 0.1 in (a) and (c), 0.4 in (b) and(d); black for $w = 0$, red for $w < 0$.

reducing the direct effect of the diabatic heating on temperature (Q/ϵ), the temperature perturbation is larger, and the fraction of global energy stored as thermal energy increases, which reduces the kinetic energy (i.e. further reduces the divergent kinetic energy and moderates the increase in the rotational kinetic energy).

As the diffusive effect of energy transport on temperature is larger for small horizontal extents L_x and L_y of the diabatic heating than for large extents, the reduction of this effect with increasing y_0 is stronger for small L_x and L_y (Figs 1b,d and 2b,d) than for large extents (Figs 1a,c and 2a,c).

In the off-equatorial Gill circulation, the gyre near the diabatic-heating maximum and the associated temperature maximum exhibit a similar sensitivity to the latitude of the diabatic heating y_0 as in the damped inertio-gravity wave (Fig. 3). In particular, the off-equatorial westerly jet becomes faster. The gyre in the other hemisphere and the equatorial, Kelvin-like easterlies weaken with increasing y_0, which can be attributed to decrease the amplitude of diabatic heating in the equatorial region with increasing y_0. But the vertical motion is much less sensitive to y_0 than in the damped inertio-gravity wave (Fig. 4), particularly for small horizontal extents of the diabatic heating. In this off-equatorial Gill circulation, subsidence is preferentially west and poleward of the heating maximum, and more so for large y_0 and large extents of the heating.

3.2 Overturning circulation

As in Part I, we investigate the intensity of overturning circulation, because of its relevance to the coupling between dynamics and the hydrologic cycle. We define the intensity of the overturning circulation Γ as the upward vertical mass flux integrated over the horizontal domain (which, by mass conservation, is the same as the downward vertical mass flux integrated over the domain):

$$\Gamma = \iint_{w>0} w \, dx \, dy. \tag{30}$$

Γ can be computed numerically using the expression of w in Equation (20) above and Equations (30)-(32) from Part I.

Figure 5a shows the intensity Γ of the overturning circulation for the f-plane case, as a function of the characteristic latitudinal extent L_y and the latitude y_0 of the center of the heating. In all cases, the longitudinal extent of the heating is still proportional to the latitudinal extent: $L_x = 3L_y$, so that L_y controls the horizontal extent of the diabatic heating in both directions. For the damped inertio-gravity wave, Γ decreases with both L_y and y_0, in a similar fashion except along the axes. For $y_0 = 0$, the sensitivity of Γ is that of the damped gravity wave studied in Part I (the decrease with L_y corresponds to the decrease along the diagonal of Figure 5a in Part I). In Section 2.2, we established that the ascending motion's asymptote in the limit $L_y \to 0$ is the diabatic heating: $w \sim Q$, and it follows that $\Gamma \sim [Q]$, independent of the heating-center latitude y_0, as in the case of the damped gravity wave and the equatorial Gill circulation (see Part I). For large latitude $y_0 = 2$ and extent $L_y = 2$, Γ is 90% smaller than its value for $L_y = 0$. Compared to Γ for the damped gravity wave (case $y_0 = 0$), Γ for the damped inertio-gravity wave is the same for $L_y = 0$ but much smaller for large L_y, as illustrated in Figure 5b.

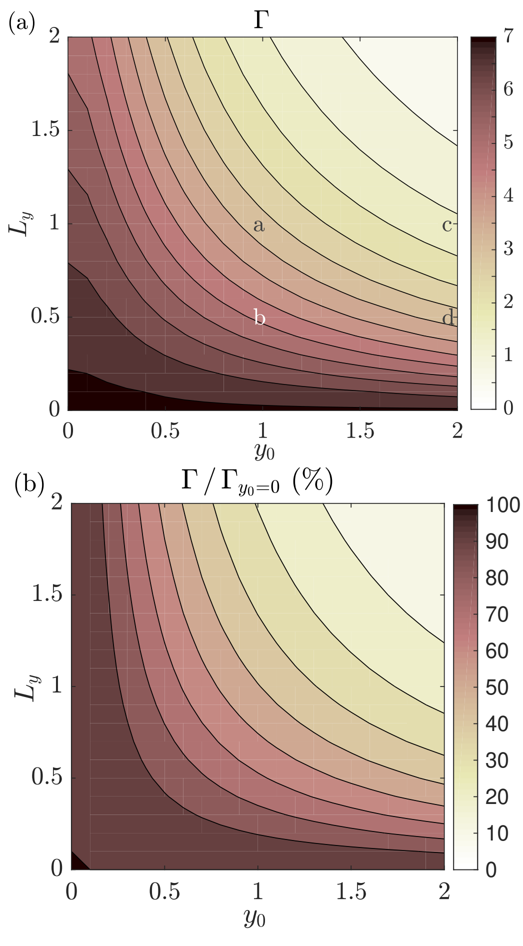

Figure 5: (a) Intensity Γ of the overturning circulation in the f-plane case; the letters "a", "b", "c", and "d" indicate the cases shown in Figures 1 and 2; (b) Ratio of Γ to its value in the non-rotating case $y_0 = 0$ (in % of $\Gamma(y_0 = 0)$); in all cases, $L_x = 3L_y$.

These sensitivities are a direct consequence of the changes in w commented in the previous section (see also Fig. 2): w is smaller for larger L_y and larger f because of the smaller transport feedback on the direct, local temperature response Q/ϵ to diabatic heating Q, which results in a smaller difference $w = Q - \epsilon T$. This smaller vertical speed w translates into a weaker overturning circulation Γ through spatial integration, although it is unclear how the region of ascent changes with L_y and y_0. Figure 2 illustrates this point: the longitude/latitude aspect ratio of the ascending region appears to change with y_0.

Figure 6a shows the intensity Γ of the overturning circulation for the β-plane case, as a function of the latitude of the heating center y_0 and the characteristic horizontal extent of the heating L_y (still with $L_x = 3L_y$). For this off-equatorial Gill circulation, Γ decreases with L_y by up to 60% as in the equatorial case (for $y_0 = 0$, analyzed in detail in Part I). Γ also decreases slightly with y_0; Figure 6b shows Γ as a percentage of its value in the equatorial case (for $y_0 = 0$), which confirms that Γ only decreases by at most 15% for y_0 going from 0 to 2. For $L_y \to 0$, Γ is independent of y_0; as we established in Section 2.2, $w \sim Q$, and $\Gamma \sim [Q]$ in this limit, as in the equatorial case, in the damped inertio-gravity and gravity waves.

Part I shows that, in the equatorial case, Γ is less intense for the Gill circulation than for the damped gravity wave for L_x and $L_y > 0$. The corresponding analysis for the off-equatorial case is to compare Γ for the Gill circulation and for the damped inertio-gravity wave. Figure 6c shows their ratio, and we find the sensitivity analyzed in Part I along the axis $y_0 = 0$. For diabatic heating close to the equator, Γ is more intense in the damped inertio-gravity wave than in the Gill circulation; but Γ decreases fast with increasing y_0 (for $L_y \neq 0$) for the damped inertio-gravity while it decreases only slightly for the Gill circulation. As a result the overturning circulation of the Gill circulation becomes larger than for the damped inertio-gravity wave for a threshold in y_0 between 0.3 and 0.7, depending on the value of L_y (see thick black line in Fig. 6c). For small y_0, the Coriolis parameter f is small and the effect of rotation as well: the damped inertio-gravity wave is very similar to the damped gravity wave; for the same y_0, the Gill circulation includes very significant rotational effect because the non-dimensional Coriolis parameter $y/2$ is significant away from the equator and as a result Γ is smaller than in the damped inertio-gravity wave. For large y_0, the β effect disrupts the regular gyre of the damped inertio-gravity wave: the winds react differently to the temperature gradients south and north of the diabatic heating and β convergence distorts the symmetry of the temperature field through vertical advection. Following energy considerations detailed in the previous section, this yields a weaker rotational wind for the off-equatorial Gill circulation than for the damped inertio-gravity wave, and a faster divergent wind associated with a more intense overturning circulation.

Figure 4 suggests that most of the upward motion is limited to a region between $-L_x$ and L_x in longitude, with a meridional extent that scales with L_y, as in Part I. We find that Γ can be approximated by the integral Γ_* of w over the domain ($[-L_x,L_x]$,$[y_0 - 4L_y, y_0 + 4L_y]$), with the latitudinal bounds corresponding to twice the e-folding distance of D:

$$\Gamma \approx \Gamma_* = \int_{y^-}^{y^+} \int_{-L_x}^{L_x} w \, dx \, dy, \tag{31}$$

with $y^- = y_0 - 4L_y$ and $y^+ = y_0 + 4L_y$. Approximating Γ by Γ_* introduces an error which is small for most of the domain of (y_0,L_y) values considered here, but it is significant, up to 20% for extended diabatic heating away from the equator (large L_y and y_0). This approximation allows us to analyze the contribution of the different cylinder modes to the sensitivity of the overturning circulation; it can be decomposed in a series:

$$\Gamma_* = \sum_{n=0}^{\infty} \Gamma_*^{(n)} = \sum_{n=0}^{\infty} \Gamma_*^{(n,1)} + \Gamma_*^{(n,2)}, \tag{32}$$

with $\Gamma_*^{(n,1)}$ and $\Gamma_*^{(n,2)}$ the contributions of the first and second part of the response to the projection of the diabatic heating Q on the n^{th} cylinder function D_n, i.e., a_n multiplied by the response to a diabatic heating in the form $F(x)D_n(y)$.

$$\Gamma_*^{(n,i)} = a_n \int_{y^-}^{y^+} \int_{-L_x}^{L_x} w^{(n,i)}\, dx\, dy, \tag{33}$$

for $i = 1, 2$. Appendix A shows that we can write these contributions as:

$$\Gamma_*^{(n,1)} = \gamma_n(L_x) f_n(y_0, L_y) + [1 - \gamma_{2n}(L_x)]\, g_{n,1}(y_0, L_y) \tag{34}$$

$$\Gamma_*^{(n,2)} = \gamma_{n+2}(L_x) f_n(y_0, L_y) + [1 - \gamma_{n+2}(L_x)]\, g_{n,2}(y_0, L_y) \tag{35}$$

with the variation in L_x given by the series of functions γ_n:

$$\begin{aligned}
\gamma_0 &= \tfrac{1}{2} q_0^{(0)}(L_x) &&= \frac{1}{2}\frac{1 + e^{-2\epsilon L_x}}{1 + \epsilon^2 l_x^2},\\
\gamma_1 &= 1, &&\\
\gamma_n &= \tfrac{1}{2}\frac{q_n^{(n)}(-L_x)}{n-1} = \tfrac{1}{2} q_n^{(n-2)}(-L_x) &&= \frac{1}{2}\frac{1 + e^{-2(2n-1)\epsilon L_x}}{1 + (2n-1)^2\epsilon^2 l_x^2} \text{ for } n > 0,
\end{aligned} \tag{36}$$

with $l_x = 1/k = 2L_x/\pi$; and the variation in y_0 and L_y given by:

$$f_n = a_n(L_y) I_n \text{ with } I_n = \int_{y^-}^{y^+} D_n\, dy, \tag{37}$$

$$g_{n,1} = -\frac{2n}{2n-1} a_n(L_y) \left[D_{n-1}(y^+) - D_{n-1}(y^-)\right], \text{ and} \tag{38}$$

$$g_{n,2} = \frac{2}{2n+3} a_n(L_y) \left[D_{n+1}(y^+) - D_{n+1}(y^-)\right]. \tag{39}$$

All these functions are consistent with the expressions given in Part I for $y_0 = 0$. Since $\gamma_n(0) = 1$, f_n are the values of both $\Gamma_*^{(n,1)}$ and $\Gamma_*^{(n,2)}$ for $L_x = 0$. For $L_x \to \infty$, $\gamma_n \to 0$ and $\Gamma_*^{(n,i)} \to g_{n,i}$ for $i = 1, 2$. We also have $I_1 = -2\left[D_0(y^+) - D_0(y^-)\right]$, which yields $g_{1,1} = f_1$.

Since $\gamma_n(0) = 1$, $\Gamma_*^{(n,i)} = f_n$ for all n and $i = 1, 2$ in the limit $L_x \to 0$, and we can establish by integration that Γ_* is an excellent approximation of Γ (as in the equatorial case):

$$\Gamma_*(0, L_y, y_0) = 2\int_{y^-}^{y^+} \sum_{n=0}^{\infty} a_n D_n\, dy = 2\int_{y^-}^{y^+} D\, dy = 4\sqrt{\pi}\,\mathrm{erf}(2) = \mathrm{erf}(2)[Q], \tag{40}$$

which is independent of y_0 and a good approximation of $\Gamma(0, L_y, y_0) = [Q]$.

Figures 7 shows some functions $\gamma_n(L_x)$ (for n even, these functions are also shown in Figure 8a of Part I). All but γ_1 tend to zero for $L_x \to \infty$, and their decay is faster for larger n. For all $n \neq 1$, $\Gamma_*^{(n,i)}$ decreases from f_n for $L_x = 0$ to $g_{n,i}$ for $L_x \to \infty$ (with $i = 1, 2$). They converge faster towards their asymptotes for larger n; this is explained in Part I by the increasing effect of rotation on circulations forced by diabatic heating along cylinder functions D_n of increasing n, which have maxima increasingly far from the equator in regions of increasingly large Coriolis parameter. The increasing effect of rotation weakens the overturning circulation and increases the temperature perturbation. γ_1 is an exception: it is constant as a result of the zero temperature perturbation: $T^{(n,1)} = 0$, independent of L_x. This means that the contribution $\Gamma_*^{(1,1)}$ will vary exclusively with L_y and y_0.

Figures 8-10 show the functions f_n, $g_{n,1}$, and $g_{n,2}$ for $n \leq 5$. The functions f_{2n}, $g_{2n,1}$, and $g_{2n,2}$ shown in Figure 8c-d of Part I correspond to the axis $y_0 = 0$ in the first column of Figures 8-10. For small y_0 and/or large L_y, the intensity of the simulation is dominated by the contributions for $n = 0$ since f_0 is significantly larger than the other f_n, and γ_0 and γ_2 make the contributions of the two components decay slowly towards $g_{0,1} = 0$ and $g_{0,2}$ (Figs. 7, 8a, and 10a); this is similar to the equatorial case. For larger y_0 and $L_y < 1$, the contributions for $n = 1$ become dominant instead, and more so for large L_x since $\gamma_1 = 1$ is constant (Figs. 7, 8b, and 10b). But the modes with larger n do contribute to the sensitivity of Γ to L_x, L_y, and y_0. Note that the limit of Γ_* for $L_x \to 0$ gives us a constraint on the sum of all f_n: $\sum_{n=0}^{\infty} f_n = \mathrm{erf}(2)[Q]$, independent of L_y and y_0. For $n > 1$, we can distinguish the domain $L_y \leq 1$ from the $L_y > 1$.

- For $L_y > 1$: for n odd, f_n, $g_{n,1}$, and $g_{n,2}$ decay rapidly towards zero as L_y increases (Figs. 8c-f, 9c-f, and 10c-f): this is a result of the decrease of a_n with increasing L_y and the fact that the D_n with n odd are odd functions of y, and compensations between the positive and negative segments of D_n contribute to reduce I_n. For n even, f_n are similar to the case $y_0 = 0$ (see Part I for details): they increase from zero at $L_y = 1$, reach a maximum and slowly decrease to zero for $L_y \to \infty$. The maximum value of f_n decreases with n and the value of L_y at which f_n reaches this maximum increases with n. As the sum of all f_n is constant, this means the decrease of f_0 with increasing L_y is compensated by f_n with increasingly large n. For $L_x > 0$, the contributions from these modes decrease like γ_n and γ_{n+2}, which decrease faster for larger n, and as a result the decrease of Γ_* with increasing L_x is faster for larger L_y, and creates a decrease of Γ_* with L_y for $L_x > 0$. In this range of L_y, this decrease is very similar across the range of y_0 under consideration. To summarize, an increase in L_y results in larger projections of D onto cylinder functions D_n with larger n, which cause dynamical responses that are weaker in terms of divergent circulation due to the increasing influence of rotation.
- For $L_y \leq 1$, the influence of modes with $n > 1$ is complex, with multiple compensations, and there is a stronger sensitivity to y_0. A few points can be made:
  - For all y_0, we can see that all $f_n \geq 0$ for small L_y, and it is zero if y_0 is a root of D_n. This is because the projection coefficient a_n is proportional to the cylinder function D_n for $L_y \to 0$:

    $$a_n \approx \frac{\sqrt{2}}{n!} D_n(y_0),$$

    and we have the following asymptotes:

    $$I_n \sim 8 D_n(y_0) L_y \quad \text{and} \quad f_n \sim \frac{8\sqrt{2}}{n!} D_n(y_0)^2 L_y \geq 0.$$

    In the limit $L_x \to 0$, all modes contribute positively to Γ_* for small L_y. The asymptotes of functions $g_{n,1}$ and $g_{n,2}$ are proportional to $D_n(y_0)$, so they are zero for values of y_0 (among others) that also cancel f_n.
  - In the small-to-intermediate range of y_0, for $n > 1$, the integral I_n changes within an interval of L_y included in $]0\,1[$ because the sign of the function D_n is opposite to $D_n(0)$ for most of the interval $[y^- \, y^+]$. In terms of sensitivity to L_x and L_y, this causes large compensations between modes and between components of the modes in terms of sensitivity. For small y_0, it is very similar to the equatorial case (see Part I for details), with all $g_{n,1}$ and $g_{n,2}$ contributing positively to Γ_* in the limit $L_x \to \infty$; furthermore $g_{n,1} > f_n$ and $g_{n,2} < f_n$, which means that the contributions $\Gamma_*^{n,1}$ decrease the sensitivity of Γ_* to L_x while the con-

tributions $\Gamma_*^{n,2}$ decrease this sensitivity: there is a compensation between the contributions of the two components' gyres to the divergent circulation.

– For large y_0 (larger than the largest root of D_n), $D_n \sim y^n \exp -y^2/4$ is positive over the interval $[y^-, y^+]$, so its integral I_n is positive. We also have:

$$a_n \sim \frac{{y_0}^n}{n!(L_y^2+1)^n}\sqrt{\frac{2}{L_y^2+1}} \quad > \quad 0,$$

which yields $f_n = a_n I_n \geq 0$ for all L_y. I_n, and therefore f_n, increases for increasing small L_y (with $I_n = 0$for $L_y = 0$) and a_n, and therefore f_n, tends to zero for large L_y. This asymptotic behavior is visible within the range of y_0 plotted in Figure 8 for $n \leq 3$. For these large values of y_0, D projects increasingly on D_n of larger n (since a_n scales with ${y_0}^n$), and its sensitivity to the horizontal extent increases due to the larger influence of rotation on the dynamical response to heating along D_n with larger n.

Despite this overall complexity, it appears clearly that the two components of the cylinder modes $n = 0$ and $n = 1$ are the main contributors to Γ_*, because of large f_n, small $g_{n,2}$, and because γ_n decreases slowly (or not at all) with L_x. For mode $n = 0$, Kelvin-wave and Rossby-wave pattern both contribute to convergence in the region of heating. For mode $n = 1$, the first component is exclusively divergent and contributes to a large part of the cross equatorial flow. For $n > 1$ the sensitivity of the first and second components $\Gamma_*^{(n,1)}$ and $\Gamma_*^{(n,2)}$ partially offset each other for small L_y.

Thanks to the continuity equation, we can also decompose Γ_* into the sum of a contribution from the meridional wind (v integrated over the boundary at $y = y^{\pm}$ and a contribution Γ_{*u} from the zonal wind (u integrated over the boundaries at $x = \pm L_x$). And each contribution $\Gamma_*^{(n,i)}$ can also be decomposed in the same way:

$$\Gamma_* = \Gamma_{*u} + \Gamma_{*v} \quad \text{and} \quad \Gamma_*^{(n,i)} = \Gamma_{*u}^{(n,i)} + \Gamma_{*v}^{(n,i)}$$

Because $u^{(0,1)}(-L_x) = 0$ and $u^{(n,i)}(L_x) = 0$ for all $n > 0$ or i=2, the contribution from the zonal wind at the eastern border results exclusively from the damped Kelvin wave extending eastward from the heating, while the contribution from the zonal wind at the western border results from a combination of damped Rossby waves. By integrating u using Equations (24)-(31) in Part I, we can write:

$$\Gamma_{*u}^{(n,1)} = \gamma_n(L_x)\left[f_n(y_0, L_y) - (2n-1)g_{n,1}(y_0, L_y)\right], \tag{41}$$
$$\Gamma_{*u}^{(n,2)} = \gamma_{n+2}(L_x)\left[f_n(y_0, L_y) + (2n+3)g_{n,2}(y_0, L_y)\right], \tag{42}$$

and we can obtain Γ_{*u} by summing over n. Note that $\Gamma_{*u}^{(1,1)} = 0$, as expected, since $f_1 = g_{1,1}$. Figure 6d shows that Γ_{*u} is the dominant contribution to Γ_*, above 90% for most of the parameter range under consideration, and even slightly above 100% for a significant parameter range, with little sensitivity to y_0. As in the equatorial case, the contribution Γ_{*v} from the meridional wind is small and can be negative, as shown in Figure 6f because of the compensation between the branches of the gyres in opposite directions. Within the contribution of the zonal wind, we can distinguish that of the damped Kelvin wave $\Gamma_{*u}^{(0.1)}$, which is also the contribution from the eastern boundary at $x = L_x$. Figure 6e shows that $\Gamma_{*u}^{(0.1)}$ is negligible for small L_y; this is consistent with the asymptote for $L_x \to 0$ (see Eq. (29), with $L_x = 3L_y$) in which the zonal wind is zero at $x = L_x$. It increases with increasing L_y, up to 60% of Γ_* for large L_y where it becomes larger than the contribution from the western boundary (above 60% of Γ_*). While the meridional contribution Γ_{*v} to Γ_* is small and in places negative (see Fig. 6f), the contribution $\Gamma_{*v}^{(1,1)}$ of the purely meridional flow for $n = 1$ is positive and Figure 6g shows that it can account for a significant fraction (up to 50%) of Γ_* for heating away from the equator.

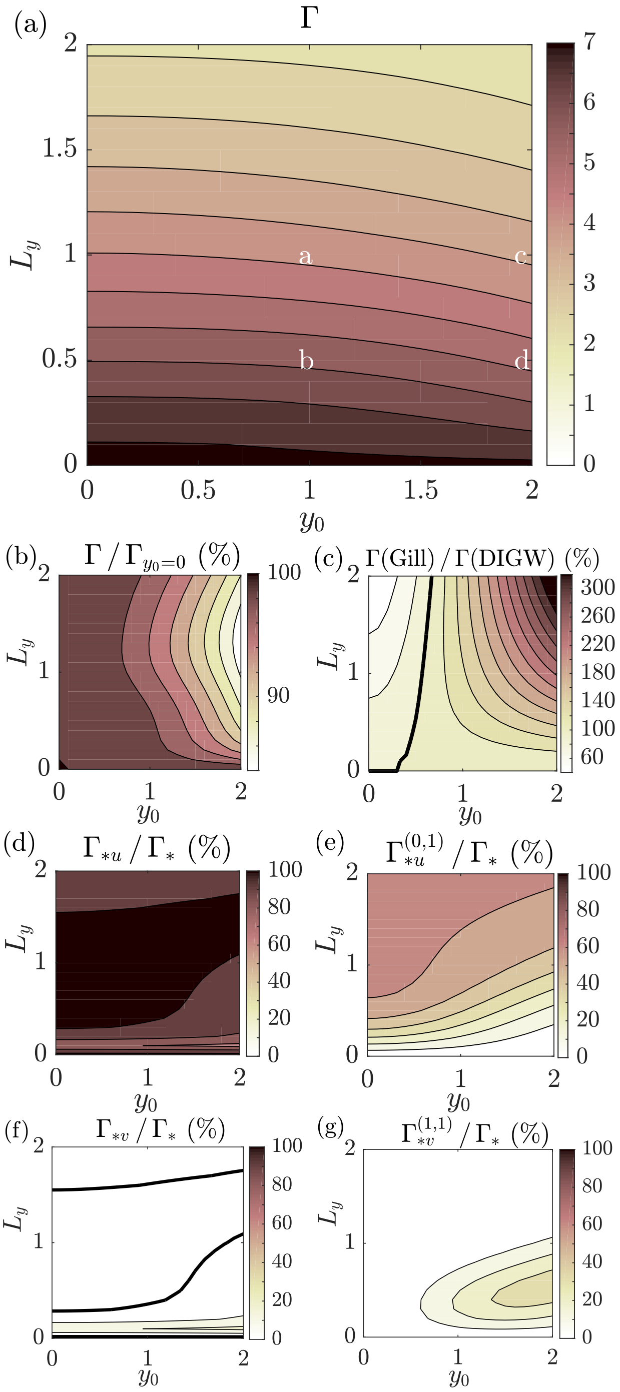

Figure 6: (a) Intensity Γ of the overturning circulation for the β-plane case; the letters "a", "b", "c", and "d" indicate the cases shown in Figures 3 and 4; (b) Ratio of this intensity to that in the equatorial case (($y_0 = 0$); (c) Ratio of the intensity of the overturning circulation in the β-plane case to that in the f-plane case; (d) Contribution Γ_{*u} of the zonal flow to the approximated overturning circulation Γ_* (in % of Γ_*); (e) Contribution $\Gamma^{(0,1)}_{*u}$ of the easterly flow to the approximated overturning circulation Γ_* (in % of Γ_*); (f) Contribution Γ_{*v} of the meridional flow to the approximated overturning circulation Γ_* (in % of Γ_*); and (g) Contribution $\Gamma^{(1,1)}_{*v}$ of the first component of the mode $n = 1$ (purely meridional flow) to the approximated overturning circulation Γ_* (in % of Γ_*); in all cases, $L_x = 3L_y$.

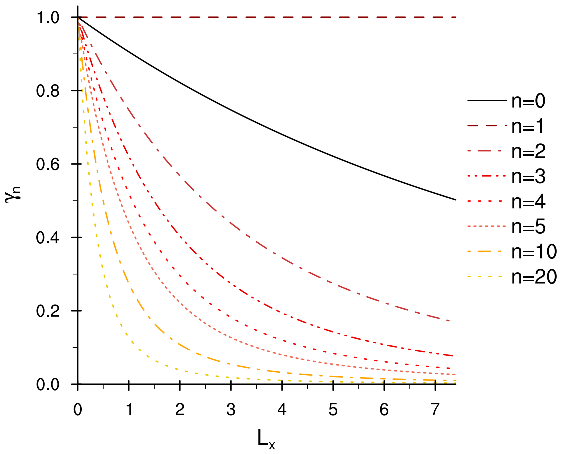

Figure 7: Functions γ_n determining the sensitivity of the contribution $\Gamma_*^{(n,i)}$ to the longitudinal extent L_x of the diabatic heating for $n \leq 5$, $n = 10$, and $n = 20$.

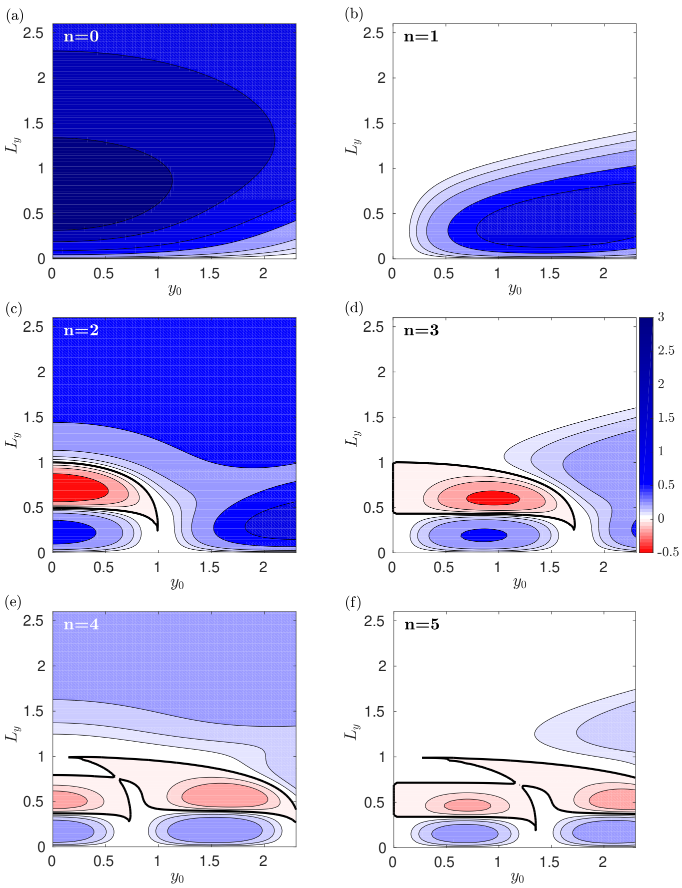

Figure 8: Functions f_n determining the sensitivity of $\Gamma_*^{(n,i)}$ ($i = 1, 2$) in the limit for $L_x = 0$ to the latitude of the y_0 of the diabatic heating and its latitudinal extent L_y, for $n \leq 5$.

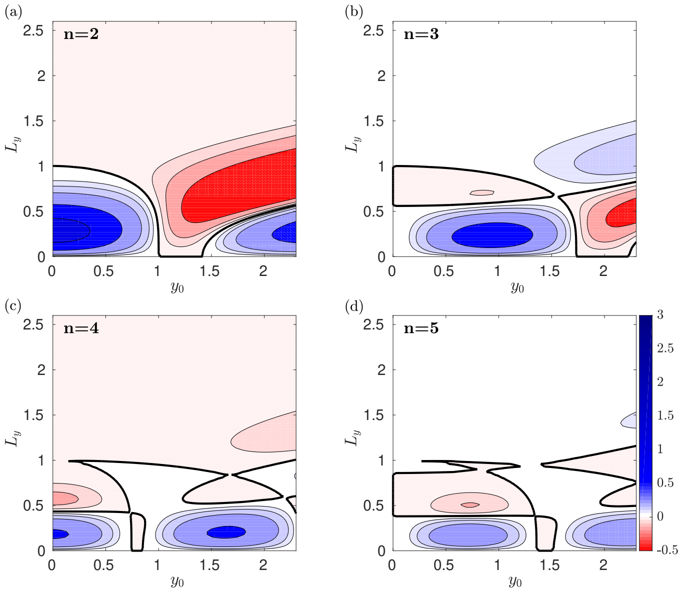

Figure 9: Functions $g_{n,1}$ determining the sensitivity of $\Gamma_*^{(n,1)}$ in the limit for $L_x \to \infty$ to the latitude of the y_0 of the diabatic heating and its latitudinal extent L_y, for $n \leq 5$. $g_{0,1} = 0$ and $g_{1,1} = f_1$ are not shown.

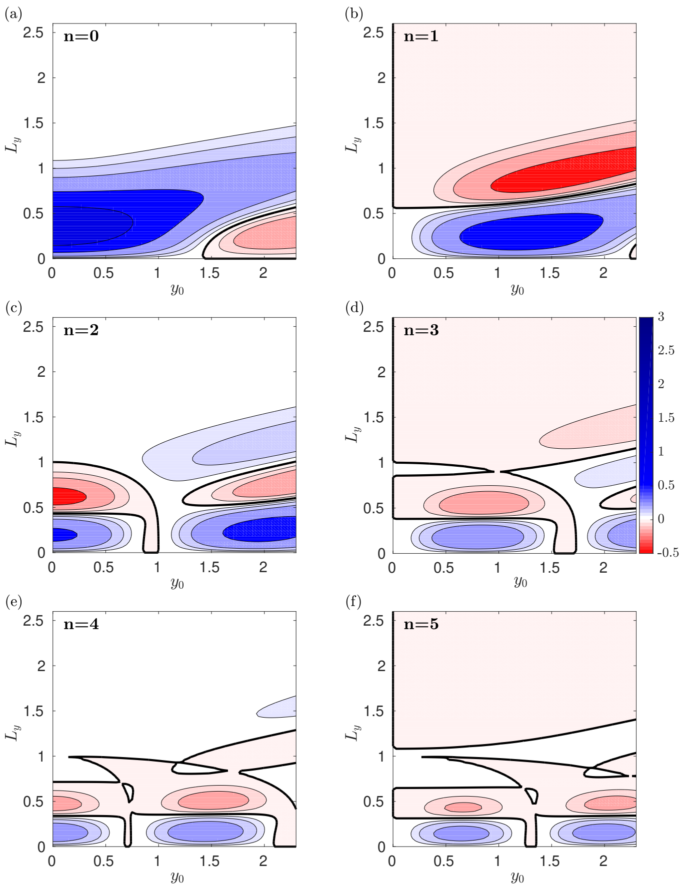

Figure 10: Functions $g_{n,2}$ determining the sensitivity of $\Gamma_*^{(n,2)}$ in the limit for $L_x \to \infty$ to the latitude of the y_0 of the diabatic heating and its latitudinal extent L_y, for $n \leq 5$.

3.3 Equatorial westerly jet

While the damped inertio-gravity wave has no horizontal wind at the center of the diabatic heating, the β effect creates a low-level westerly jet in the Gill circulation. If a coupling with surface thermodynamics is activated, this jet will decrease the surface turbulent heat fluxes if the background surface wind is easterly, for example in trade winds; it will increase the surface fluxes if the background wind is westerly, in the equatorial the Indian Ocean or in monsoon jets. The resulting modulation of surface fluxes has been pointed out as a potential energy source for tropical intraseasonal variability (Bellon & Sobel, 2008a, 2008b; Sobel et al., 2008, 2010) and a important mechanism for their coupling with the surface ocean (Maloney & Sobel, 2004; Bellon et al., 2008). In the off-equatorial case, the westerly jet is not symmetric with respect to the central latitude of the diabatic heating (see Fig. 3), it results mainly from the cyclonic circulation around the heating and reaches its maximum equatorward of the heating maximum. As can be seen in Figure 3, as the horizontal scale of the heating decreases, the main gyre becomes smaller and faster, which accelerates the low-level westerly jet; as the latitude of the heating increases, the jet accelerates as well.

The low-level westerly wind u_{o} at the center of the heating was studied in details for the equatorial case in Part I; for the off-equatorial case, its sensitivity to the latitude of the heating center y_0 is small and its sensitivity to the horizontal extent of the heating L_x and L_y is similar to the equatorial case (see Fig 9a in Part I). This is consistent with wind-induced turbulent surface fluxes acting as an energy source for disturbances in regions of mean westerlies. But u_{o} is not as relevant in the off-equatorial case as in the equatorial case: while in that case u_{o} is the maximum westerly wind on the y-axis, in the off-equatorial case this maximum wind u_{M} is equatorward of the heating center. Figure 11a shows the sensitivity of this maximum wind: it increases with the latitude y_0 of the center of diabatic heating, but mostly it increases with decreasing horizontal extent L_y, and tends towards infinity for $L_y \to 0$. Part I showed that, for $y_0 = 0$, $u_{\mathrm{M}} = u_{\mathrm{o}} \sim 2/L_y$; Appendix B shows that u_{M} diverges faster for $y_0 \neq 0$:

$$u_{\mathrm{M}} \sim \frac{1}{\sqrt{2\mathrm{e}}} \frac{y_0}{{L_y}^2}. \tag{43}$$

Figure 11b shows the latitudinal shift of this maximum low-level westerly wind along the y-axis ($u_{\mathrm{M}} = u(0, y_0 + y'_{u_{\mathrm{M}}})$). For large L_y (> 1), the latitude of the wind maximum is mostly sensitive to y_0: the further poleward the center of heating, the further the wind maximum from the center of heating. For small L_y, the latitude of the wind maximum is mostly sensitive to L_y: it converges towards y_0 for very small L_y (Appendix B shows that $y'_{u_{\mathrm{M}}} \sim -\sqrt{2}L_y$ for $L_y \to 0$).

As in Part I, we also investigate the integrated intensity of the jet $U = -\int_{u<0} u(0, y)dy$, the longitudinal extent of the jet x_u along the x-axis, and characteristic latitudinal extent of the jet y_u along the y-axis. Because the jet is not symmetric in latitude with respect to the center of heating, the latitudinal extent y_u is the average between the poleward and equatorward extents:

$$y_u = \frac{1}{2}\left({y_u}^+ - {y_u}^-\right), \text{ with } u(0, {y_u}^-) = u(0, {y_u}^+) = 0 \text{ and } {y_u}^- < y_0 < {y_u}^+.$$

In addition, we introduce a measure of the asymmetry of the jet, the equatorward asymmetry index E_u, which measures how much more than half the jet is equatorward of the heating center ($E_u = 0$ corresponds to a jet symmetric about the latitude y_0 of the heating center, $E_u = 1$ to a jet entirely equatorward of the heating center):

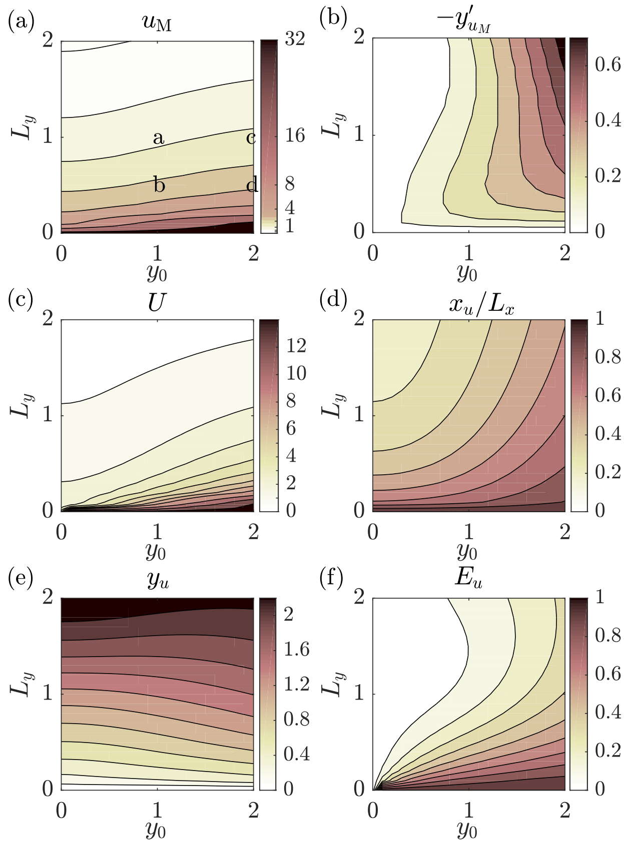

Figure 11: Characteristics of the equatorial westerly jet in the Gill circulation: (a) maximum westerly zonal velocity u_{M} on the y-axis ; the letters "a", "b", and "c" indicate the cases shown in Figures 3 and 4; (b) equatorward latitudinal shift $-y'_{u_{\mathrm{M}}}$ of the maximum westerly zonal velocity; (c) intensity U of the jet; (d) zonal extent x_u of the jet normalized by L_x; (e) meridional extent y_u of the jet; (f) equatorward asymmetry index E_u of the jet.

$$E_u = 2\,\frac{y_0 - {y_u}^-}{y_u} - 1.$$

Figure 11c shows the sensitivity of the intensity U of the jet to y_0 and L_y. The sensitivity of U is similar to that of u_{M}, with an increase of U with increasing y_0, but mostly an increase of U with decreasing L_y. For $L_y \to 0$, U is finite if $y_0 = 0$ (see Part I), but if $y_0 \neq 0$, $U \sim y_0/L_y$ (see Appendix B), which tends towards infinity. Figure 11e shows the latitudinal extent y_u of the jet along the y-axis; it is not very sensitive to y_0 and scales roughly with the horizontal extent L_y of the heating for moderate and large values of L_y. For $L_y \to 0$, Appendix B shows that this linear scaling breaks down: $y_u \sim L_y\sqrt{-2\ln L_y}$. Compared to the equatorial case in which the scaling of the maximum wind $u_{\mathrm{M}} =\sim 2/L_y$ and that of the latitudinal extent of the jet $y_u \sim 2L_y$ provide a finite upper bound for U, in the off-equatorial case there is no such upper bound: both the scaling of the wind maximum $u_{\mathrm{M}} \sim y_0/(\sqrt{2\mathrm{e}}{L_y}^2)$ and that of the jet's latitudinal extent $y_u \sim L_y\sqrt{-2\ln L_y}$ increase faster or decrease slower with decreasing L_y than in the equatorial case, and both effects explain the divergence of U for $L_y \to 0$. The scaling of y_u results from the slow convergence of the equatorward boundary ${y_u}^-$ of the westerly jet towards y_0 for $L_y \to 0$, as can be seen from the asymmetry index E_u in Figure 11f: $E_u \to 1$ for $y_0 \neq 0$ and $L_y \to 0$, which means that the jet extends exclusively equatorward of y_0 in this limit. The jet is symmetric ($E_u = 0$) in the equatorial case ($y_0 = 0$), and the asymmetry of the jet increases with increasing y_0. It also decreases with increasing L_y for small L_y, but this sensitivity becomes non-linear at larger L_y.

Finally, Figure 11d shows the eastward longitudinal extent x_u along the x-axis of the low-level westerly jet, normalized by L_x. For small L_y (and L_x, since the ratio L_x/L_y is fixed), $x_u \approx L_x$, which means that the westerly jets extends over the whole region of diabatic heating at the equator, irrespective of y_0 (see Appendix B). x_u/L_x decreases with L_y but more so in the equatorial case than in the off-equatorial case: for $y_0 = 2$, this decrease is twice slower than for $y_0 = 0$

In summary, compared to the equatorial case presented in Part I, the low-level westerly jet in the off-equatorial case:

- has about the same latitudinal extent y_u except for small horizontal extents of the diabatic heating for which y_u does tend towards zero for $L_y \to 0$, but slower than in the equatorial case;
- is about as fast at the heating center, but faster at its maximum wind speed, and causes a larger low-level eastward mass transport. These differences are markedly larger for small horizontal extents of the diabatic heating;
- is asymmetric with respect to the latitude of the heating center y_0, extending further equatorward than poleward, with its maximum wind speed equatorward of the heating center. For small horizontal extents of the diabatic heating, the jet is almost exclusively equatorward of the heating center;
- extend further eastward than in the equatorial case.

In terms of sensitivity to the horizontal extent of the heating, the difference is significant in terms of the normalized longitudinal extent of the westerly jet (same limit for $L_y \to 0$, but less sensitivity to increasing L_y) and in terms of the maximum speed u_M and intensity U for small horizontal scales (larger scaling for $L_y \to 0$).

4 Summary and Conclusion

In this article, we explore the scale sensitivity of the off-equatorial Gill circulation (Part I studies the equatorial case), keeping the horizontally-integrated diabatic heating fixed in order to understand how the spatial spread of the diabatic heating influences the dynamical response of the tropical atmosphere. In our analysis, we focus on characteristics of this circulation likely to couple it with the energy cycle: intensity of the overturning circulation (linked to cloud moist processes) and characteristics of the low-level westerly flow (linked to turbulent surface heat fluxes). We also compare our solutions to the dynamical response on an f-plane, which is a damped inertio-gravity wave.

We find that the intensity of the overturning circulation Γ decreases slightly with increasing latitude of the diabatic-heating center y_0, except for very small horizontal extent of the heating for which it is independent of y_0 and the same as in the damped (inertio-)gravity wave. In other words, the sensitivity of Γ to the horizontal extent of the heating increases slightly with y_0. Compared to the inertio-gravity wave response, the Gill circulation is much less sensitive to y_0 for non-zero horizontal extent of the diabatic heating. As a result, for y_0 below a fairly low threshold Γ for the Gill circulation is more sensitive to the horizontal extent of the diabatic heating, and therefore smaller, than for the damped inertio-gravity wave, as in the equatorial case (see Part I); but above this threshold, Γ for the Gill circulation is less sensitive to the horizontal extent of the diabatic heating, and therefore larger, than for the damped inertio-gravity wave (see Fig. 6c). In the equatorial or near equatorial cases, the β effect introduces some effect of rotation which creates rotational circulations. As argued in Part I and Section 3.1 from an energy perspective, the conversion of thermal energy to kinetic energy in rotational circulations is at the expense of the divergent circulation and reduces the overturning circulation. In off-equatorial cases, the same effect of rotation is particularly apparent in the damped inertio-gravity wave, with a strong rotational circulation symmetric with respect to the heating center. In these cases, the β effect breaks the symmetry by causing accelerations that are not symmetric with respect to the heating center, create secondary divergent circulations, and weaken the rotational circulation to the benefit of the overall divergent circulation.

The overturning circulation results mostly from the convergence of the zonal wind, with a large contribution of the Kelvin-wave component for large-scale diabatic heating. The meridional contribution tend to be small and can be negative, despite a significant positive contribution of the meridional-only, $n = 1$, component for significantly off-equatorial diabatic heating. Also, the region of ascent is less and less colocated with the region of diabatic heating as the latitude of the heating increases. Overall the sensitivity of the Gill circulation indicates that its coupling with the hydrologic cycle would create a weaker moisture-convergence feedback in the off-equatorial case compared to the equatorial case.

The low-level westerly jet intensifies as the diabatic heating is shifted poleward. At the same time the position of maximum wind respective to the heating center shifts equatorward. For small-scale heating, the jet extends entirely equatorward of the heating center, its latitudinal extent is very small, its maximum speed and the eastward low-level mass transport tend to infinity. This sensitivity of the low-level westerly jet is consistent with the monsoon low-level jet (Joseph & Raman, 1966) being faster than the equatorial westerlies in the Indian Ocean during other seasons. It also explains the large intraseasonal variability of this monsoon jet (Joseph & Sijikumar, 2004) in response to the intraseasonal variability of convection. The low-level westerly jet impacts turbulent surface fluxes, increasing them in westerlies and decreasing them in easterlies, and the intensity of this jet suggests a large impact. The combination of the seasonal monsoon jet and an intraseasonal westerly jet south of northward-propagating convective disturbances has been suggested as a growth mechanism for the boreal-summer monsoon intraseasonal oscillation (Bellon & Sobel, 2008a, 2008b; Sobel et al., 2010) and as a large component of its coupling with the ocean (Sengupta et al., 2001; Roxy & Tanimoto, 2007; Bellon et al., 2008; Gao et al., 2019, among others). Our results suggest that, over mean westerlies, the wind-induced surface fluxes are larger and extend to a larger fraction of the heating region for small convective disturbances than for large convective disturbances, favoring the development of small disturbances. And the sensitivity of these wind-induced surface fluxes to the increasing latitude of the diabatic heating is similar to the sensitivity to decreasing horizontal extent of the heating, except for their latitudinal extent. But the influence of this jet and its sensitivity on convective disturbances is not straightforward: the region of westerlies is increasingly asymmetric with respect to the heating center with decreasing horizontal extent of the diabatic heating, which favors equatorward propagation of a convective disturbance or slows poleward propagation in westerlies. The complex combination of sensitivities should have some bearings on the development, scale, and propagation of monsoon intraseasonal oscillation events worthy of further investigation.

Appendix A Sensitivity to the Aspect Ratio L_x/L_y

This appendix investigates the sensitivity of the integrated metrics of the overturning circulation and the low-level westerly jet Γ and U to changes in the aspect ratio of the diabatic-heating region. Since isolines of heating are close to circular for $L_x = 3L_y$, which is the case discussed in the main text, we set $L_x = 3aL_y$ and document the sensitivity of our main results to a. Figure A1 shows the ratio of the intensity Γ of the overturning circulation in the off-equatorial case to its intensity in the equatorial case ($y_0 = 0$) for different aspect ratios of the heating region: $a = 1/2$ (Fig. A1a) and $a = 2$ (Fig. A1b); the case $a = 1$ is shown in Figure 6b. It appears that the sensitivity of Γ to the latitude of the heating varies little with the aspect ratio of the region of heating. In all cases, the intensity of the overturning circulation for $L_x \to 0$ is $\Gamma = [Q]$, independent of both L_y and y_0; for large L_x and L_y, the normalized decrease of Γ with increasing y_0 is similar in all cases. There is one difference in the scale for which this decrease with y_0 is fastest: while it is for $L_y \approx 1.3$ for $a = 1/2$, it is for a smaller $L_y \approx 0.5$ for $a = 2$.

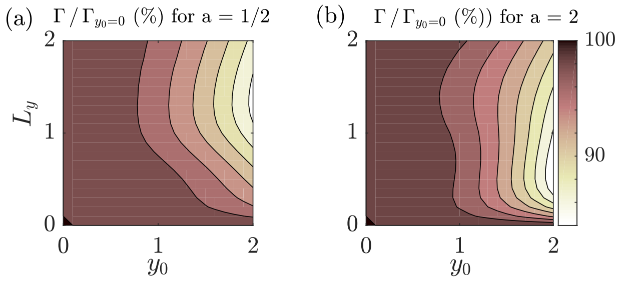

Figure A1: Ratio of the intensity Γ of the overturning circulation in the off-equatorial case to its intensity in the equatorial case ($y_0 = 0$) for (a) $a = 1/2$ and (b) $a = 2$ ($L_x = 3aL_y$); the case $a = 1$ is shown in Figure 6b.

Figure A2 shows that the sensitivity of the intensity of the westerly mass transport U exhibits a very similar sensitivity to the latitude of the heating y_0. The normalized increase of U with y_0 is essentially independent from a.

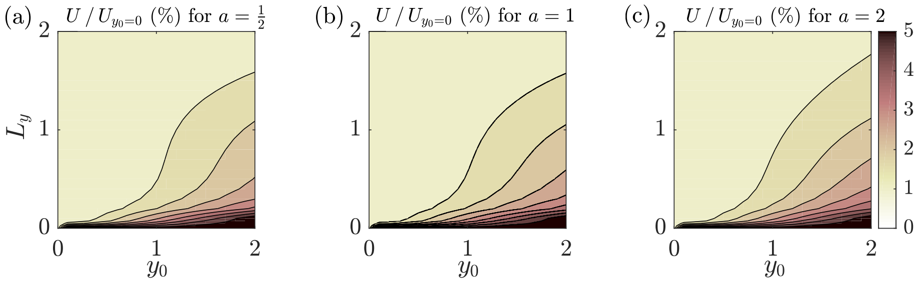

Figure A2: Ratio of the intensity U of the low-level westerly jet in the off-equatorial case to its intensity in the equatorial case ($y_0 = 0$) for (a) $L_x = 1.5L_y$, (b) $L_x = 3L_y$, and (c) $L_x = 6L_y$.

Appendix B Contributions of the Cylinder Modes to Γ_*

By using the expressions of $w^{(n,i)}$ ($i = 1$ or 2) (Eq. (32) in Part I) combined with the expressions of $T^{(n,i)}$ (Eqs. (30) and (31) in Part I), we can write $\Gamma_*^{(n,i)}$ as:

$$\Gamma_*^{(n,1)} = \frac{a_n}{2}\left(\int_{-L_x}^{L_x} F\,dx\; I_n - \epsilon\int_{-L_x}^{L_x} q_n^{(n)}\,dx\;\left[I_n + nI_{n-2)}\right]\right), \tag{B1}$$

$$\Gamma_*^{(n,2)} = \frac{a_n}{2}\left(\int_{-L_x}^{L_x} F\,dx\; I_n - \epsilon\int_{-L_x}^{L_x} q_{n+2}^{(n)}\,dx\;\left[I_{n+2} + (n+2)I_n\right]\right), \tag{B2}$$

for all n. We have introduced the notation $I_n = \int_{y-}^{y+} D_n\,dy$ for $n \geq 0$ and $I_{-1} = I_{-2} = 0$.

The integral of F is 2 and the differential Equations (18) and (21) in Part I yield the following expressions for the integrals of the functions $q_{n(+2)}^{(n)}$:

$$\epsilon\int_{-L_x}^{L_x} q_0^{(0)}\,dx = 2 - q_0^{(0)}(L_x), \tag{B3}$$

$$\epsilon\int_{-L_x}^{L_x} q_1^{(1)}\,dx = 0, \tag{B4}$$

$$\epsilon\int_{-L_x}^{L_x} q_n^{(n)}\,dx = \frac{1}{2n-1}\left[2n - 2 - q_n^{(n)}(-L_x)\right] \quad \text{for } n > 1, \tag{B5}$$

$$\text{and } \epsilon\int_{-L_x}^{L_x} q_{n+2}^{(n)}\,dx = \frac{1}{2n+3}\left[2 - q_{n+2}^{(n)}(-L_x)\right] \quad \text{for all } n, \tag{B6}$$

in which we have used $q_0^{(0)}(-L_x) = 0$, $q_1^{(1)} = 0$, $q_n^{(n)}(L_x) = 0$ for $n > 1$, and $q_{n+2}^{(n)}(L_x) = 0$ for all n.

Equation (A6) in Part I yields:

$$I_{n-2} = \frac{1}{n-1}\left(I_n + 2\left[D_{n-1}(y^+) - D_{n-1}(y^-)\right]\right) \quad \text{and} \quad I_{n+2} = (n+1)I_{2n} - 2\left[D_{n+1}(y^+) - D_{n+1}(y^-)\right] \tag{B7}$$

Using Equations (B3)-(B7), Equations (B1) and (B2) can be rewritten:

$$\Gamma_*^{(0,1)} = \frac{q_0^{(0)}(L_x)}{2}a_0 I_0, \tag{B8}$$

$$\Gamma_*^{(1,1)} = a_1 I_1, \tag{B9}$$

$$\Gamma_*^{(n,1)} = \frac{q_n^{(n)}(-L_x)}{2n-2}a_n I_n - \frac{2n}{2n-1}a_n\left[D_{n-1}(y^+) - D_{n-1}(y^-)\right]\left(1 - \frac{q_n^{(n)}(-L_x)}{2n-2})\right) \quad \text{for } n > 1, \tag{B10}$$

$$\Gamma_*^{(n,2)} = \frac{q_{n+2}^{(n)}(-L_x)}{2}a_n I_n + \frac{2}{2n+3}a_n\left[D_{n+1}(y^+) - D_{n+1}(y^-)\right]\left(1 - \frac{q_{n+2}^{(n)}(-L_x)}{2})\right) \quad \text{for all } n, \tag{B11}$$

By replacing $q_n^{(n)}$ by its expressions (Eqs. (24)-(26) in Part I), and using $q_n^{(n)} = (n-1)q_n^{(n-2)}$, $\Gamma_*^{(n,i)}$ can be written as in Equations (34) and (35).

The contribution $\Gamma_{*u}^{(n,i)}$ to $\Gamma_*^{(n,i)}$ from the zonal flow is simply the integral of the zonal velocity $u^{(n,i)}$ over the zonal boundary of the the rectangle $(2L_x, 8L_y)$ where it is not zero, multiplied by $\pm a_n$. Using the expressions of $u^{(n,i)}$ (Eqs. (24)-(31) in Part I), it can be written as:

$$\Gamma_{*u}^{(0,1)} = \frac{a_0}{2} q_0^{(0)}(L_x) I_0 = \Gamma_*^{(0,1)}, \tag{B12}$$
$$\Gamma_{*u}^{(1,1)} = 0, \tag{B13}$$
$$\Gamma_{*u}^{(n,1)} = -\frac{a_n}{2} q_n^{(n)}(-L_x)\left[I_n - nI_{n-2}\right] \quad \text{for } n > 1, \tag{B14}$$
$$\Gamma_{*u}^{(n,2)} = -\frac{a_n}{2} q_{n+2}^{(n)}(-L_x)\left[I_{n+2} - (n+2)I_n\right] \quad \text{for all } n. \tag{B15}$$

The last two can be simplified into (using Eq. (A6) in Part I):

$$\Gamma_{*u}^{(n,1)} = \frac{q_n^{(n)}(-L_x)}{2n-2} a_n \left(I_n + 2n\left[D_{n-1}(y^+) - D_{n-1}(y^-)\right]\right) \quad \text{for } n > 1, \tag{B16}$$
$$\Gamma_{*u}^{(n,2)} = \frac{q_{n+2}^{(n)}(-L_x)}{2} a_n \left(I_n + 2\left[D_{n+1}(y^+) - D_{n+1}(y^-)\right]\right) \quad \text{for all } n. \tag{B17}$$

By replacing $q_n^{(n)}$ by its expression from Equations (24)-(26) in Part I, and using $q_n^{(n)} = (n-1)q_n^{(n-2)}$, $\Gamma_{*u}^{(n,i)}$ can be written as in Equations (41) and (42).

Appendix C Characteristic of the Jet for $L_y \to 0$

In this appendix, we focus on the limit of the solution for L_y (and L_x) $\to 0$ in the off-equatorial case ($y_0 \neq 0$). From Equation (29), which gives the expression of the zonal baroclinic wind field for $L_x \to 0$, it is clear that along the x axis, the zonal wind is negative (westerly in the low-troposphere) for $x \leq x_u$, with:

$$x_u = \frac{1}{k} \arcsin\left(1 - \frac{a_0}{2} L_y\right) \to L_x \text{ for } L_y \to 0, \tag{C1}$$

since $a_0 \to \sqrt{2}\exp\left(-\frac{y_0^2}{4}\right)$ and $k = \pi/2Lx$.

Along the y-axis, the baroclinic zonal wind can be written:

$$u(0,y) = -2\left(1 - \frac{y(y-y_0)}{4{L_y}^2}\right) D(y) + a_0 D_0(y); \tag{C2}$$

for $L_y \to 0$, it is westerly around the heating center ($u_\mathrm{o} < 0$) and it is easterly for $y = 0$. There is no straightforward solution for the latitude of sign change or maximum of $u_{x=0}$. But we can see that for small L_y the westerly jet becomes narrow and close to y_0, so we can look for solutions in the form of a asymptotic development:

$$y' = \sum_{n=1}^{\infty} b_n {L_y}^n, \tag{C3}$$

For $u(0,y) = 0$, this yields one solution:

$${y_u}^+ = y_0 + \frac{4}{y_0} {L_y}^2 - \frac{2\sqrt{2}}{y_0} \mathrm{e}^{-\frac{y_0^2}{2}} {L_y}^3 + \mathcal{O}\left({L_y}^4\right), \tag{C4}$$

and it is unsuccessful to determine ${y_u}^-$ (because $yy' < 0$ in the range of y of interest, and the first parenthesis on the right-hand side in Eq. (C2) is always larger than 1). By a careful study of the scalings of the different terms in Equations (C2), we can find the following asymptotic solution:

$$y_u{}^- = y_0 - 2\sqrt{2}L_y\left(\mathcal{L} + \frac{1}{4\mathcal{L}}\left[\ln\left(\mathcal{L}y_0\right) + \frac{y_0^2}{2}\right]\right), \tag{C5}$$

with $\mathcal{L} = \sqrt{-\ln L_y}$.

For $L_x \to 0$, we can obtain an expression for U using Equation (26) to integrate $u(0, y)$ by parts over the interval $[y_u{}^-\ y_u{}^+]$: And we will have:

$$U = y_u{}^+ D\left(y_u{}^+\right) - y_u{}^- D\left(y_u{}^-\right) + \sqrt{\pi}\left[\operatorname{erf}\left(\frac{y_u'{}^+}{2L_y}\right) - \operatorname{erf}\left(\frac{y_u'{}^-}{2L_y}\right) + a_0 \operatorname{erf}\left(\frac{y_u{}^+}{2}\right) - a_0 \operatorname{erf}\left(\frac{y_u{}^-}{2}\right)\right], \tag{C6}$$

and taking the limit for $L_y \to 0$ (using the asymptotic development of $y_u{}^+$ and $y_u{}^-$ above), we get:

$$U = \frac{y_0}{L_y} - \sqrt{\pi} + \mathcal{O}\left(\mathcal{L}L_y\right). \tag{C7}$$

As for the maximum westerly wind, it is located at $y = y_{u_\mathrm{M}}$ where:

$$0 = \frac{du(0, y}{dy} = \frac{1}{2L_y{}^2}\left[3y' + y\left(1 - \frac{y'^2}{2L_y{}^2}\right)\right]D(y) - \frac{a_0}{2}yD_0(y), \tag{C8}$$

in which we used $y' = y - y_0$ for simplicity.

Looking for an asymptotic expansion following Equation (C3), we find:

$$y_{u_\mathrm{M}} = y_0 - \sqrt{2}L_y + \frac{3}{y_0}L_y{}^2 + \frac{3\sqrt{2}}{4y_0{}^2}L_y{}^3 + \left[2\exp\left(\frac{1}{2} - \frac{y_0{}^2}{4}\right) - \frac{12}{y_0{}^3}\right]L_y{}^4 + \mathcal{O}\left(L_y{}^5\right), \tag{C9}$$

which yields:

$$u_\mathrm{M} = \frac{1}{\sqrt{2\mathrm{e}}}\frac{y_0}{L_y{}^2} - \frac{2}{\sqrt{\mathrm{e}}L_y} - \frac{1}{2\sqrt{2\mathrm{e}}y_0} - \sqrt{2}\mathrm{e}^{-\frac{y_0^2}{2}} + \mathcal{O}\left(L_y\right). \tag{C10}$$

Acknowledgments

The authors thank Jean-Philippe Duvel for his useful comments. The authors also acknowledge the support of the University of Auckland, and particularly financial support from its Faculty of Science in the form a PhD fellowship and a grant from the Faculty Research Development Fund. G.B. is also supported by the Glavish-Buckley Lectureship.

References

Bellon, G. (2011). Monsoon intraseasonal oscillation and land-atmosphere interaction in an idealized model. *Climate Dynamics*. doi: 10.1007/s00382-010-0893-0

Bellon, G., & Sobel, A. (2010). Multiple equilibria of the hadley circulation in an intermediate-complexity axisymmetric model. *Journal of Climate*, *23*, 1760–1778.

Bellon, G., & Sobel, A. H. (2008a). Instability of the axisymmetric monsoon flow and intraseasonal oscillation. *Journal of Geophysical Research: Atmosphere*, *113*, D07108. doi: 10.1029/2007JD009291

Bellon, G., & Sobel, A. H. (2008b). Poleward-propagating intraseasonal monsoon disturbances in an intermediate-complexity axisymmetric model. *Journal of the Atmospheric Sciences*, *65*, 470–489.

Bellon, G., Sobel, A. H., & Vialard, J. (2008). Ocean-atmosphere coupling in the monsoon intraseasonal oscillation: a simple model study. *Journal of Climate*, *21*, 5254–5270.

Bellon, G., & Srinivasan, J. (2006). Comment on "Structures and mechanisms of the northward propagating boreal summer intraseasonal oscillation". *Journal of Climate*, *19*, 4738–4743.

Boos, W. R., & Kuang, Z. (2010). Mechanisms of poleward propagating, intraseasonal convective anomalies in cloud system–resolving models. *Journal of the Atmospheric Sciences*, *67*(11), 3673–3691.

Cauchy, A. L. B. (1821). *Cours d'analyse de l'École Royale Polytechnique: Analyse algébrique. I.re partie.* Paris: Debure frères.

Gao, Y., Klingaman, N. P., DeMott, C. A., & Hsu, P.-C. (2019). Diagnosing ocean feedbacks to the bsiso: Sst-modulated surface fluxes and the moist static energy budget. *Journal of Geophysical Research: Atmospheres*, *124*(1), 146–170.

Gill, A. E. (1980). Some simple solutions for heat-induced tropical circulation. *Quarterly Journal of the Royal Meteorological Society*, *106*(449), 447–462. doi: 10.1002/qj.49710644905

Goswami, B. N. (2005). South Asian monsoon. In W. K. M. Lau & D. E. Waliser (Eds.), *Intraseasonal variability in the atmosphere-ocean climate system* (pp. 19–61). Springer, Berlin, Heidelberg.

Jiang, X., Li, T., & Wang, B. (2004). Structures and mechanisms of the northward propagating boreal summer intraseasonal oscillation. *Journal of Climate*, *17*, 1022–1039.

Joseph, P. V., & Raman, P. L. (1966). Existence of low level westerly jet stream over peninsular india during july. *Indian J Meteorol Geophys*, *17*(1), 407–410.

Joseph, P. V., & Sijikumar, S. (2004). Intraseasonal variability of the low-level jet stream of the asian summer monsoon. *Journal of Climate*, *17*(7), 1449-1458. doi: 10.1175/1520-0442(2004)017⟨1449:IVOTLJ⟩2.0.CO;2

Kang, I.-S., Kim, D., & Kug, J.-S. (2010). Mechanism for northward propagation of boreal summer intraseasonal oscillation: Convective momentum transport. *Geophysical Research Letters*, *37*(24).

Maloney, E., & Sobel, A. H. (2004). Surface fluxes and ocean coupling in the tropical intraseasonal oscillation. *Journal of Climate*, *17*, 4368–4386.

Ramage, C. S. (1971). *Monsoon meteorology.* Academic Press New York.

Reboredo, B., & Bellon, G. (2020). Scale sensitivity of the gill circulation, Part I: equatorial case. *Journal of Advances in Modeling Earth Systems*, submitted.

Roxy, M., & Tanimoto, Y. (2007). Role of SST over the Indian ocean in influencing the intraseasonal variability of the Indian summer monsoon. *Journal of the Meteorological Society of Japan*, *85(3)*, 349–358.

Sengupta, D., Goswami, B. N., & Senan, R. (2001). Coherent intraseasonal oscillations of ocean and atmosphere during the Asian summer monsoon. *Geophysical Research Letters*, *28*, 4127–4130.

Sharmila, S., Pillai, P., Joseph, S., Roxy, M., Krishna, R., Chattopadhyay, R., ... Goswami, B. (2013). Role of ocean–atmosphere interaction on northward propagation of indian summer monsoon int ra-seasonal oscillations (miso). *Climate dynamics*, *41*(5-6), 1651–1669.

Sobel, A. H., Maloney, E. D., Bellon, G., & Frierson, D. M. (2008). The role of surface heat fluxes in tropical intraseasonal oscillations. *Nature Geoscience*, *1*(10), 653–657.

Sobel, A. H., Maloney, E. D., Bellon, G., & Frierson, D. M. (2010). Surface fluxes and tropical intraseasonal variability: A reassessment. *Journal of Advances in Modeling Earth Systems*, *2*, 2. doi: 10.3894/JAMES.2010.2.2

Sobel, A. H., & Neelin, J. D. (2006). The boundary layer contribution to intertropical convergence zones in the quasi-equilibrium tropical circulation model framework. *Theoretical and Computational Fluid Dynamics*, *20*(5-6), 323–350. doi: 10.1007/s00162-006-0033-y

Wu, G. X., Liu, Y., Zhu, X., Li, W., Ren, R., Duan, A., & Liang, X. (2009). Multiscale forcing and the formation of subtropical desert and monsoon. *Annales Geophysicae*, *27*(9), 3631–3644. doi: 10.5194/angeo-27-3631-2009